responsible for shifting the resonant frequencies of solar p-modes can be used to locate images of active regions on the far side of the sun when these modes are treated from the local optical perspective of seismic holography. Therefore, the far-side images reinforce a growing consensus (*20, 21*) that reduced sound-travel times in active regions may explain the entirety of the frequency shifts of global p-modes with the solar cycle.

The application of seismic holography to active regions on the far side of the sun makes it possible to study how active regions absorb, emit, and scatter low-ℓ waves. Plain acoustic power holography of near-side active regions renders both sunspots and plages with strong egression power deficits, comparable in significance to the phase shifts. Acoustic power holography of far-side active regions renders an unexpectedly weak signature, which is not clearly detectable in our computations. Therefore, we see that the deficit in acoustic noise radiating from plages (*6, 22, 23*) is substantially selective in favor of high-ℓ p-modes. This remarkable development seems tentatively consistent with recent work that attributes the acoustic egression deficit of waves emanating from magnetic regions to the coupling of p-modes with slow Alfvèn modes (*24, 25*). Low-ℓ p-modes are characterized by mostly vertical motion, and thus couple only weakly to vertical magnetic fields.

References and Notes

1. C. Lindsey and D. C. Braun, *Sol. Phys.* **126**, 101 (1990).
2. D. C. Braun *et al.*, *Astrophys. J.* **392**, 739 (1992).
3. C. Lindsey *et al.*, in *GONG 1992: Seismic Investigation of the Sun and Stars* (Astronomical Society of the Pacific, San Francisco, CA, 1993), pp. 81–84.
4. D. C. Braun *et al.*, *Astrophys. J.* **335**, 1015 (1988).
5. T. J. Bogdan *et al.*, *Astrophys. J.* **406**, 723 (1993).
6. D. C. Braun, *Astrophys. J.* **451**, 859 (1995).
7. C. Lindsey and D. C. Braun, *Astrophys. J.* **485**, 895 (1997).
8. F. Roddier, *C. R. Hebd. Seances Acad. Sci. Ser. B* **281**, 993 (1975).
9. J. Christensen-Dalsgaard *et al.*, *Astrophys. J.* **403**, L75 (1993).
10. C. Lindsey and D. C. Braun, *Sol. Phys.*, in press; see §3, equation 1, therein.
11. Plages are magnetic regions whose flux densities, ranging from 100 to 1200 G, are considerably greater than those of the quiet sun (up to 100 G) but considerably less than those of sunspots (1200 to 3000 G). Plages viewed near the center of the solar disk are nearly invisible against the quiet sun in white light, but near the limb are about 5% brighter than the quiet sun. The strong magnetic fields of sunspots visibly depress their umbrae more than 200 km beneath level of the quiet photosphere. The reduced travel times of plages may be the result of a similar, but smaller, depression by their weaker magnetic fields.
12. T. L. Duvall Jr. *et al.*, *Nature* **362**, 430 (1993).
13. T. L. Duvall Jr. *et al.*, *Nature* **379**, 235 (1996).
14. P. H. Scherrer *et al.*, *Sol. Phys.* **162**, 129 (1995).
15. See §4 in (*10*).
16. The National Oceanic and Atmospheric Administration (NOAA), a branch of the U.S. Department of Commerce, monitors solar activity and assigns numbers to each major sunspot group. These are published in a periodical, *Solar Geophysical Data*, printed monthly by NOAA.
17. D. C. Braun and C. Lindsey, *Sol. Phys.*, in press.
18. The National Solar Observatory (NSO) operates solar telescopes at the Kitt Peak National Observatory near Tucson, AZ, and at the Sacramento Peak Observatory near Cloudcroft, NM. NSO runs a synoptic program at the Kitt Peak Vacuum Telescope that provides daily magnetograms covering the full solar hemisphere that is directly visible from the Earth. These are made available at www.nso.noao.edu/diglib.
19. Supplemental material is available at www.sciencemag.org/feature/data/1047789.shl.
20. R. Howe *et al.*, *Astrophys. J.* **524**, 1084 (1999).
21. B. W. Hindman *et al.*, *Sol. Phys.*, in press.
22. C. Lindsey and D. C. Braun, *Astrophys. J.* **499**, L99 (1998).
23. D. C. Braun, *et al.*, *Astrophys. J.* **502**, 968 (1998).
24. P. S. Cally and T. J. Bogdan, *Astrophys. J.* **486**, L67 (1997).
25. P. S. Cally, *Sol. Phys.*, in press.

26. We greatly appreciate the support we have gotten from P. Scherrer, an early and enthusiastic proponent of far-side imaging, and from the SOHO SOI-MDI team. SOHO is a project of international cooperation between the European Space Agency and NASA. Supported by NSF grants ATM-9214714 and AST-9528249, by NASA grant NAG5-7236, and by a research contract, PY-0184, sponsored by Stanford University.

8 December 1999; accepted 3 February 2000

Extreme Oxygen Sensitivity of Electronic Properties of Carbon Nanotubes

Philip G. Collins,* Keith Bradley, Masa Ishigami, A. Zettl†

The electronic properties of single-walled carbon nanotubes are shown here to be extremely sensitive to the chemical environment. Exposure to air or oxygen dramatically influences the nanotubes' electrical resistance, thermoelectric power, and local density of states, as determined by transport measurements and scanning tunneling spectroscopy. These electronic parameters can be reversibly "tuned" by surprisingly small concentrations of adsorbed gases, and an apparently semiconducting nanotube can be converted into an apparent metal through such exposure. These results, although demonstrating that nanotubes could find use as sensitive chemical gas sensors, likewise indicate that many supposedly intrinsic properties measured on as-prepared nanotubes may be severely compromised by extrinsic air exposure effects.

Many carbon materials have excellent molecular adsorption and sieving properties (*1*). Carbon nanotubes in particular, because of their size, large surface area, and hollow geometry, are being considered as prime materials for gas adsorption (*2–4*), Li storage (*5, 6*), and selective molecular filtering (*7, 8*). Independently, the results of numerous theoretical and experimental studies suggest that single-walled carbon nanotubes (SWNTs) behave as nearly ideal one-dimensional quantum wires (*9–12*). However, virtually no attention has been given to the possible interdependence of gas adsorption and electrical quantum conductance in nanotubes, despite the large surface area of these materials.

We show here that the measured electronic properties of nanotubes [electrical resistance R, thermoelectric power S, and local density of states $N(E)$] are in fact exceedingly sensitive to environmental conditions, namely gas exposure (*13*), and can be reversibly "tuned" simply by exposure to air or oxygen. Isolated, apparently semiconducting nanotubes can be converted into apparent metals through room-temperature exposure to oxygen. Hence the electronic properties of a given nanotube are not specified only by the diameter and chirality of the nanotube but depend critically on gas exposure history. Because virtually all previous experimental studies of SWNTs have used samples exposed to air (and perhaps to other contaminants as well from aqueous solution purification or cutting processes), the results of those measurements must be carefully reevaluated before firm conclusions are drawn, especially with respect to the theoretically predicted behavior of idealized pure nanotubes.

The SWNTs used in our experiments were grown by the conventional laser ablation method (*14*). Material from different synthesis runs yielded similar results. In general, SWNT-rich material taken directly from the growth chamber was baked in air at 700°C to remove the majority of amorphous and microcrystalline carbon. In determining both transport and spectroscopy characteristics, different additional sample preparation and contacting procedures were used and compared in order to quantify nanotube modifications that might arise, for example, from the commonly used practices of ultrasound exposure, filtering, and surfactant addition.

Measurements of the dc electrical resistance R and thermoelectric power (TEP) S

Department of Physics, University of California at Berkeley, and Materials Sciences Division, Lawrence Berkeley National Laboratory, Berkeley, CA 94720, USA.

*Present address: IBM T. J. Watson Research Center, Post Office Box 218, Yorktown Heights, NY 10598, USA.

†To whom correspondence should be addressed. E-mail: azettl@physics.berkeley.edu

used SWNT bundles and thin films of SWNTs (*15*). The substrates were mounted in a vacuum test chamber with provisions for heating and cooling the sample and injecting different environmental gases. Resistance measurements were performed under conditions of low bias current, and the TEP was measured using a quasi-dc swept temperature gradient method with applied maximum temperature differentials of approximately 1 K, measured with miniature differential thermocouples.

Figure 1 shows R for a SWNT sample at room temperature in different gas environments, measured with a four-probe contact configuration. As the surrounding medium was cycled between vacuum ($\leq 10^{-6}$ torr) and air, a rapid and reversible change in the SWNT resistance occurred in step with the changing environment. We have repeated the experiment of Fig. 1 independently with the different major gas constituents of air and have determined that this variation in R is due to oxygen exposure. We have observed similar resistance changes at constant gas pressure by cycling the purge gas from pure dry N_2 to pure dry O_2. Oxygen-saturated SWNTs clearly have a higher electrical conductance than do SWNTs with less adsorbed oxygen.

Figure 2 shows the sensitivity of S of SWNTs to environmental gas conditions at 350 K. Initially, in a pure atmospheric pressure oxygen environment, the TEP was positive with a magnitude near +20 mV/K. This relatively large positive TEP is consistent with that reported previously for "pristine" (but air-exposed) SWNTs near room temperature (*16*). As oxygen was gradually removed from the chamber, the TEP changed continuously from positive to negative, with a final equilibrium value of approximately -10 μV/K. When oxygen was reintroduced into the chamber, the TEP again reversed sign and once again became positive. In previous analyses (*16*) of the TEP of SWNTs, it was difficult to account for the magnitude and sign of the "intrinsic" TEP without invoking charge-transfer or Kondo-impurity mechanisms. The present experiments help resolve this difficulty: as-prepared SWNTs are invariably air doped with an extrinsically induced holelike carrier concentration.

The rather dramatic 10 to 15% variation in R and change in sign of the TEP shown in Figs. 1 and 2 demonstrate that SWNTs are exceptionally sensitive oxygen sensors. Indeed, in related experiments at much lower pressures, we found measurable changes in R and TEP with changing oxygen partial pressures in gas environments as low as 10^{-8} to 10^{-10} torr.

We have repeated the R and TEP experiments of Figs. 1 and 2 at different temperatures and different sample configurations (*17*). In those experiments, the effects of oxygen exposure became increasingly more irreversible (and had longer time constants) with decreasing temperature, as expected for a gas adsorption process. In fact, our transport measurements indicate that, once SWNTs have been exposed to oxygen, it is not possible to fully deoxygenate them at room temperature even under high-vacuum conditions (for example, simply placing air-exposed SWNTs in a high-vacuum environment at room temperature does not suitably clean them; the samples must be heated in vacuum above 110° to 150°C for several hours for most of the oxygen to be desorbed). Similarly, sample topology plays an important role. Experiments performed on dilute SWNT thin films yield abrupt electronic changes with short time constants, whereas optically thick films and mats of SWNTs require higher temperatures and longer times to reach equilibrium. These observations provide strong evidence for adsorbed gas dynamics. We find that irreversible changes corresponding to possible oxygen chemisorption are observed when the transport experiments are performed at elevated temperatures (above 200°C) and over much longer times. Similar distinctions between oxygen physisorption and chemisorption are well documented for carbon fibers (*18*).

To further study the interplay between SWNT electronic properties, oxygen adsorption, and sample topology, we used the spectroscopy capabilities of a scanning tunneling microscope (STM). Previous experiments have demonstrated the utility of the STM for imaging SWNTs and determining, through scanning tunneling spectroscopy (STS), the local density of electronic states $N(E)$; both "semiconducting" and "metallic" nanotubes have been variously identified (*11*, *12*). STS is an ideal local probe of the oxygen sensitivity of individual nanotubes and complements the previously discussed spatially averaged measurements of R and TEP.

Our STS measurements were performed in a controlled gas environment, using SWNTs dispersed on conducting substrates consisting of either atomically flat Au(111) films or freshly cleaved graphite [highly oriented pyrolitic graphite (HOPG)]. Measurements were made on both single isolated SWNTs and SWNTs associated in bundles or ropes, dispersed from dichloroethane solutions to a density on the order of one nanotube or rope per square micrometer. Modest ultrasound treatment was used to obtain the isolated individual tubes. Before imaging, the SWNTs were stripped of possible contaminating adsorbates by being baked inside the STM chamber at 110°C for at least 2 hours in an inert, flowing carrier gas. The cleaned nanotubes were then cooled and initially characterized by STS while still in the inert gas environment. Different gases were subsequently bled into the STM chamber, and spectroscopy measurement of the same nanotube was continued in situ, including for different positions along the length of the tube. As a

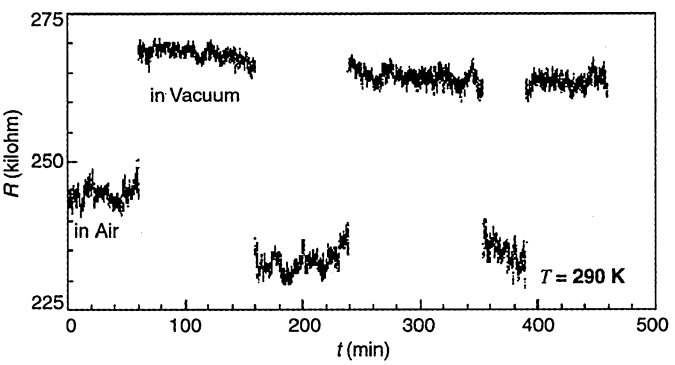

Fig. 1. Sensitivity of the electrical resistance R of SWNT films to gas exposure at a temperature (T) of 290 K. The nanotube resistance switched by 10 to 15% as the chamber surrounding the sample was alternately flooded with air or evacuated. Identical results were obtained if pure dry oxygen was used rather than air, indicating that oxygen was the source of the effect. Likewise, changing the chamber purge gas between oxygen and any inert gas resulted in similar stepwise changes in R.

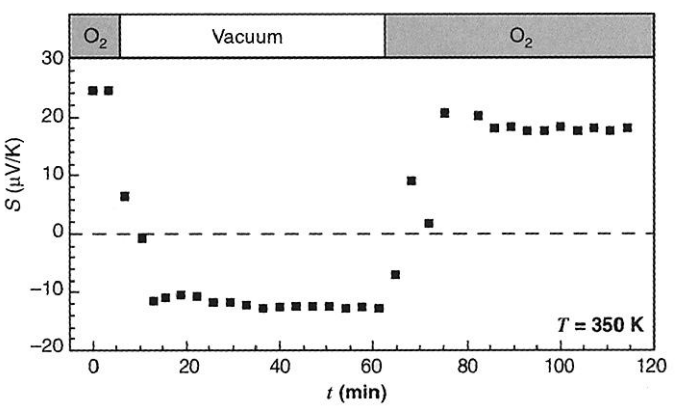

Fig. 2. Sensitivity to environmental conditions of thermoelectric power S for SWNTs at $T = 350$ K. Both the magnitude and the sign can be altered by oxygen exposure. In vacuum, S is n-type, whereas in an oxygen environment, S is p-type, with a larger magnitude. Many previous transport measurements have found that as-prepared nanotubes are strongly p-type, with no proper theoretical explanation given. Apparently such nanotubes were inadvertantly "air-doped."

check for STM tip or substrate contamination, spectroscopy was alternately performed on the tube and on the bare substrate near the nanotube. All of the measurements used a Pt-Ir tip because of its low reactivity with oxygen.

The STS results for an isolated individual SWNT (sample number 14) on a Au substrate are shown in Fig. 3, A and B. The current-voltage (*I-V*) tunneling characteristics, both in the presence of inert argon gas and after oxygen adsorption, are shown in Fig. 3A, and for comparison the gas-insensitive *I-V* of the bare Au substrate is also shown. The numerically differentiated *dI/dV* curves in Fig. 3B are roughly proportional to the local density of states $N(E)$ available for electrons tunneling from the STM tip (*19*). The *dI/dV* data indicate a clear increase in these states as the nanotube is exposed to oxygen. In fact, the inert gas–cleaned (oxygen-free) nanotube appears to have a semiconducting energy gap of roughly 0.3 eV in which no electronic states are available. Exposure to oxygen greatly alters $N(E)$, especially at negative biases, resulting in a *dI/dV* curve that is nonzero for all biases. Although some minor STS variations are observed between STS scans, the main features of these plots—that is, the significant rearrangement in $N(E)$ and a shrinking of the apparent band gap of the nanotube upon oxygen exposure—are entirely reproducible. Therefore, this nanotube has a gas exposure history–dependent $N(E)$, and after oxygen treatment it is perhaps most appropriately described as metallic (or semimetallic). The actual intrinsic behavior of the SWNT shown in Fig. 3, A and B, is not clear. STS of the tube after argon cleaning suggests a gap of roughly 0.3 eV, which is well below the conventional theoretical limits of "semiconducting" SWNTs (*20–22*). This observed small gap could be intrinsic and curvature-induced; alternatively, residual adsorbates obscure the true, larger semiconducting gap despite our cleaning procedure.

Not all of the individual SWNTs are as sensitive to oxygen exposure as that used for Fig. 3, A and B. The results of a similar experiment on a different nanotube (sample 8) (Fig. 3, C and D) show that over a substantial range in bias, $N(E)$ appears flat and zero both before and after oxygen exposure. Apparently, sample 8, a modest band-gap semiconductor, is not as sensitive to oxygen dosing as the small band-gap SWNT depicted in Fig. 3, A and B. Because of this reduced sensitivity, one might ascribe an intrinsic gap of roughly 550 meV to sample 8. We have performed STS measurements on many other SWNTs in order to ensure the reproducibility of our findings and to define overall $N(E)$ trends. We find that oxygen-induced changes in $N(E)$ are independent of the position on the tube where the data are acquired. We also find that Ar, He, and N_2 have no noticeable doping effects on the $N(E)$ of SWNTs (provided that each gas source is sufficiently dry), which is in agreement with the transport measurements discussed above.

Table 1 summarizes STS results for 17 independent SWNT samples, including the spectroscopically determined $N(E)$ after the initial inert gas bake-out and upon subsequent dry oxygen dosing, and gives the number of neighbors for a given nanotube. A single

Table 1. Summary of tunneling spectroscopy measurements on 17 different carbon nanotubes (M indicates no gap, metallic), together with the number of neighboring nanotubes. All of the samples were measured on HOPG substrates except 1 and 14, which were on Au(111) surfaces.

Sample no.	STS band gaps (mV)		Neighbors (*n*)
	Baked	O_2-exposed	
1	M	M	1–3
2	M	M	1–3
3	M	M	1–2
4	M	M	3–5
5	M	M	3–5
6	M	M	Multiple
7	M	M	Multiple
8	550	500	0–2
9	750	600	0–1
10	175	M	0–1
11	175	M	1–3
12	190	M	1–3
13	250	M	1–3
14	300	M	0
15	350	M	1–3
16	500	M	0
17	500	M	0–1

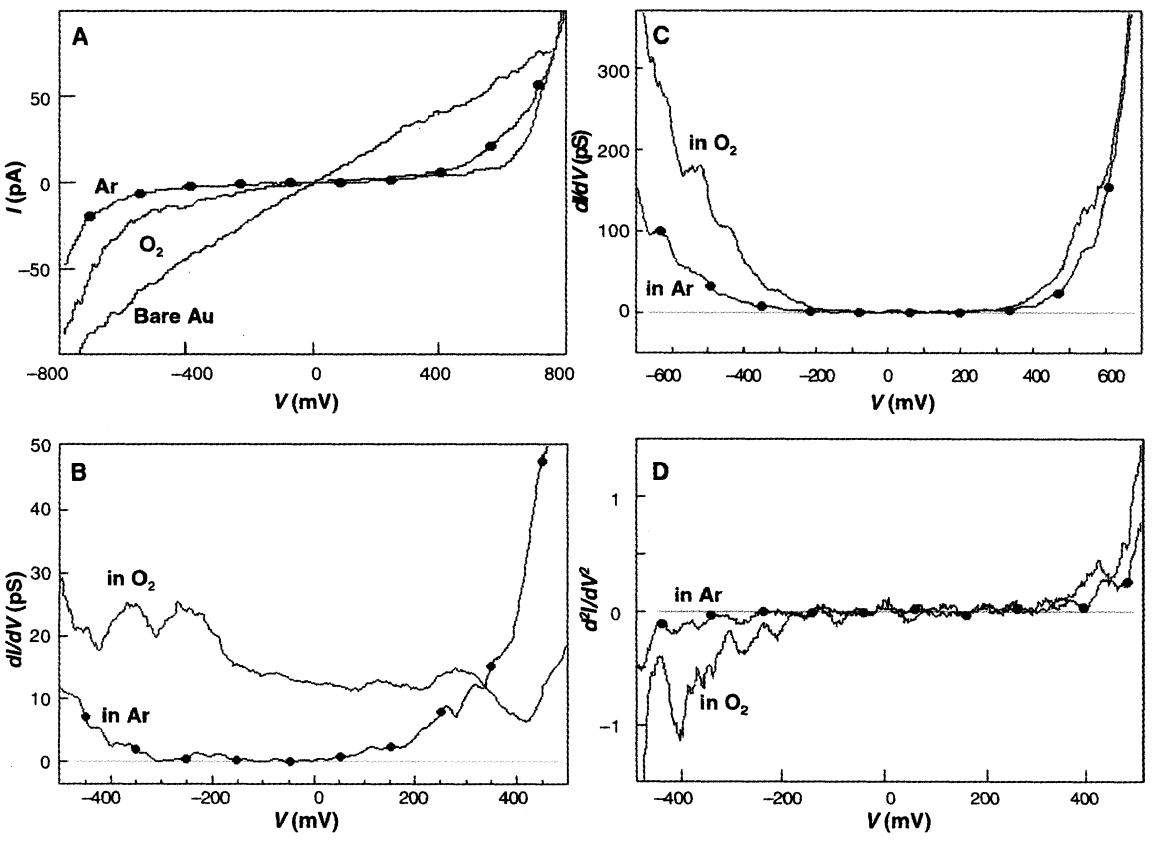

Fig. 3. (**A**) Tunneling spectroscopy *I-V* characteristics, as well as an *I-V* trace acquired over the bare Au(111) substrate, for an isolated carbon nanotube (sample 14) in inert Ar gas and after exposure to O_2. (**B**) The corresponding *dI/dV* characteristics. The nanotube is transformed from an apparent small band-gap semiconductor to an apparent metal upon exposure. (**C** and **D**) This nanotube (sample 8) was semiconducting in both Ar and O_2. O_2 exposure increased the apparent density of valence band states for $V < -200$ mV, but the actual magnitude of the band gap did not change significantly and matched theoretical predictions for a semiconducting SWNT of diameter 1.4 nm. (D) The d^2I/dV^2 curves used to define the gap.

unambiguously isolated SWNT would have zero neighbors, whereas a nanotube that is clearly part of a large bundle or rope would have multiple neighbors. The small range of neighbor numbers for some samples reflects the general difficulty in unambiguously determining this number using STM imaging alone (similarly, because of finite tip radius, sample curvature, and electronic differences between sample and substrate, using STM imaging alone it is generally difficult to accurately determine the diameter of a given nanotube). Samples 1 through 7 in Table 1 form a natural grouping: these samples were metallic both before and after oxygen dosing. The next two samples, 8 and 9, started out as modest band-gap semiconductors and they remained so. The last group, samples 10 through 17, started out as small band-gap semiconductors and became metallic upon oxygen dosing. Both isolated tubes and tubes with neighbors can be found in this last category. An interesting and suggestive (but not conclusive) observation is that all of the "intrinsically" metallic nanotubes we observed (samples 1 through 7) had nanotube neighbors; we have been unable to find an isolated SWNT that remains metallic upon inert gas cleaning.

Our transport and STS measurements can be interpreted within a consistent picture of oxygen-induced changes in the electronic behavior of SWNTs. The increases in $N(E)$ summarized in Table 1 agree with the oxygen-induced increases in conductivity we have generally measured for films or ensembles of nanotubes. If Table 1 is representative of SWNTs in general, it indicates that SWNT film conductivity might decrease by as much as 50% if all of the oxygen adsorbates could be removed. In contrast, gas adsorption studies on thin metal films generally exhibit conductivity increases as adsorbates are removed, due to surface-sensitive scattering processes (*23*). The STS data also illuminate the change in sign of the TEP. Intrinsically metallic, oxygen-free SWNTs are suggested to have a small negative TEP, whereas oxygen-exposed small band-gap SWNTs may behave as p-type, degenerately doped semiconductors with a relatively large S magnitude. For a sample that is a collection of SWNTs comprising both metals and semiconductors, the overall effects of oxygen doping on S are complex, as one must take into account not only changes in S of individual tubes but also associated changes in tube conductivity that affect the multichannel weighted average of S.

The likelihood of charge transfer from adsorbed oxygen to SWNTs deserves careful investigation. Oxygen is known to have good charge transfer to planar defected graphite, especially in the presence of catalytic metallic particles, which has made graphite the material of choice for fuel cell electrodes. Graphitic microstructures (*24*) and fibers (*18*) can both become hole-doped in the presence of adsorbed oxygen because of oxygen's electron affinity. The SWNT observations may be due to similar effects. However, a key to charge transfer between oxygen and graphite is the presence of defects (*24, 25*). If, as some studies suggest, curvature plays only a small role in adsorption and charge transfer (*26*), any oxygen-induced charge transfer in SWNTs could indicate the presence of on-tube defects, making oxygen sensitivity an ideal way to determine the concentration of defects in carbon nanotubes. In addition, the possibility that oxygen may also adsorb on the inside of nanotubes with open ends should not be overlooked.

References and Notes

1. *Graphite Intercalation Compounds II: Transport and Electronic Properties*, vol. 18, H. Zabel and S. A. Solin, Eds. (Springer-Verlag, New York, 1992).
2. A. C. Dillon *et al.*, *Nature* **386**, 377 (1997).
3. A. Chambers *et al.*, *J. Phys. Chem. B* **102**, 4253 (1998).
4. C. C. Y. Ahn *et al.*, *Appl. Phys. Lett.* **73**, 3378 (1998).
5. V. A. S. Nalimova *et al.*, *Synth. Met.* **88**, 89 (1997).
6. G. T. W. Wu *et al.*, *J. Electrochem. Soc.* **146**, 1696 (1999).
7. S. C. Tsang *et al.*, *Nature* **372**, 159 (1994).
8. K. G. Ayappa, *Langmuir* **14**, 880 (1998).
9. M. Bockrath *et al.*, *Science* **275**, 1922 (1997).
10. S. J. Tans *et al.*, *Nature* **386**, 474 (1997).
11. J. W. G. Wildoer *et. al.*, *Nature* **391**, 59 (1998).
12. T. W. Odom *et. al.*, *Nature* **391**, 62 (1998).
13. For a preliminary report, see P. G. Collins, M. Ishigami, A. Zettl, *Bull. Am. Phys. Soc.* **44**, 1889 (1999).
14. A. Thess *et al.*, *Science* **273**, 483 (1996).
15. Film samples were fabricated by depositing dichloroethane-dispersed SWNTs onto SiO_2 substrates prepatterned with gold electrodes.
16. J. Hone *et al.*, *Phys. Rev. Lett.* **80**, 1042 (1998); L. Grigorian *et al.*, *Phys. Rev. B* **60**, R11309 (1999)
17. P. G. Collins, K. Bradley, A. Zettl, in preparation.
18. N. E. Kobayashi, T. Ishii, K. Kaneko, *J. Chem. Phys.* **109**, 1983 (1998).
19. J. Tersoff and D. R. Hamann, *Phys. Rev. Lett.* **50**, 25 (1983).
20. J. W. Mintmire, B. I. Dunlap, C. T. White, *Phys. Rev. Lett.* **68**, 631 (1992).
21. N. Hamada, S. Sawada, A. Oshiyama, *Phys. Rev. Lett.* **68**, 1579 (1992).
22. M. S. Dresselhaus, G. Dresselhaus, P. C. Eklund, *Science of Fullerenes and Carbon Nanotubes* (Academic Press, New York, 1996).
23. G. Wedler, in *Thin Metal Films and Gas Chemisorption*, P. Wibman, Ed., vol. 32 of *Studies in Surface Science Catalysis* (Elsevier, New York, 1987), sections 2.4, 5.1, and 5.3.
24. L. S. Singer, in *Proceedings of the 5th Carbon Conference* (Pergamon, New York, 1961), vol. 2, pp. 37–50.
25. S. M. Lee, *et. al.*, *Phys. Rev. Lett.* **82**, 217 (1999).
26. P. J. Britto, K. S. V. Santhanam, A. Rubio, J. A. Alonso, P. M. Ajayan, *Adv. Mater.* **11**, 154 (1999).

27. We thank M. L. Cohen and S. G. Louie for useful discussions and J. Hone for help with early TEM experiments. Supported in part by a University of California, Berkeley, Chancellor's Initiative grant; by NSF grants DMR-9801738 and DMR-9501156; and by the Office of Energy Research, Office of Basic Energy Science, Materials Sciences Division of the U.S. Department of Energy under contract number DE-AC03-76SF00098. P.C. acknowledges support from a Helmholz Fellowship and M.I. acknowledges support from the Hertz Foundation.

8 December 1999; accepted 10 February 2000

Hematopoietic Stem Cell Quiescence Maintained by $p21^{cip1/waf1}$

Tao Cheng,[1] Neil Rodrigues,[1] Hongmei Shen,[1] Yong-guang Yang,[2] David Dombkowski,[1] Megan Sykes,[2] David T. Scadden[1]*

Relative quiescence is a defining characteristic of hematopoietic stem cells, while their progeny have dramatic proliferative ability and inexorably move toward terminal differentiation. The quiescence of stem cells has been conjectured to be of critical biologic importance in protecting the stem cell compartment, which we directly assessed using mice engineered to be deficient in the G_1 checkpoint regulator, cyclin-dependent kinase inhibitor, $p21^{cip1/waf1}$ (p21). In the absence of p21, hematopoietic stem cell proliferation and absolute number were increased under normal homeostatic conditions. Exposing the animals to cell cycle–specific myelotoxic injury resulted in premature death due to hematopoietic cell depletion. Further, self-renewal of primitive cells was impaired in serially transplanted bone marrow from $p21^{-/-}$ mice, leading to hematopoietic failure. Therefore, p21 is the molecular switch governing the entry of stem cells into the cell cycle, and in its absence, increased cell cycling leads to stem cell exhaustion. Under conditions of stress, restricted cell cycling is crucial to prevent premature stem cell depletion and hematopoietic death.

High levels of production of mature blood cells are needed to replace their rapid turnover, yet it has been hypothesized that the proliferative activity of hematopoietic stem cells (HSCs) is highly restricted in order to prevent susceptibility to myelotoxic insult or consumption of the regenerative cell pool (*1–3*). Once cells embark on a path of high proliferation, they appear to have longevity limited to 1 to 3 months (*4*). It has therefore been hypothesized that hematopoietic tissue is organized so that stem cells are relatively quiescent, but their more differentiat-